This Accepted Manuscript has not been copyedited and formatted. The final version may differ from this version.



Research Articles: Systems/Circuits

## Motor neurons tune premotor activity in a vertebrate central pattern generator

Kristy J. Lawton<sup>1</sup>, Wick M. Perry<sup>1</sup>, Ayako Yamaguchi<sup>2</sup> and Erik Zornik<sup>1</sup>

<sup>1</sup>Biology Department, Reed College, Portland, OR 97202

DOI: 10.1523/JNEUROSCI.2755-16.2017

Received: 31 August 2016

Revised: 5 February 2017

Accepted: 13 February 2017

Published: 20 February 2017

**Author contributions:** K.J.L., W.M.P., A.Y., and E.Z. designed research; K.J.L., W.M.P., and E.Z. performed research; K.J.L. and W.M.P. analyzed data; K.J.L. and E.Z. wrote the paper.

We thank Charlotte Barkan and two anonymous reviewers for helpful feedback on the manuscript. This work was funded by the National Institutes of Health (NS091977) and start-up funds from Reed College. The authors declare no competing financial interests.

Corresponding author: Erik Zornik 3203 SE Woodstock Blvd Portland, OR 97202 Email: ezornik@reed.edu

Cite as: J. Neurosci; 10.1523/JNEUROSCI.2755-16.2017

**Alerts:** Sign up at www.jneurosci.org/cgi/alerts to receive customized email alerts when the fully formatted version of this article is published.

Accepted manuscripts are peer-reviewed but have not been through the copyediting, formatting, or proofreading process.

<sup>&</sup>lt;sup>2</sup>Biology Department, University of Utah, Salt Lake City, UT 84112

1	Motor neurons tune premoto	or activity in a vertebrate central pattern generator
2		
3	Abbreviated title: Motor neuro	ons regulate premotor activity
4		
5	Kristy J. Lawton <sup>1</sup> , Wick M. Pe	erry <sup>1</sup> , Ayako Yamaguchi <sup>2</sup> , Erik Zornik <sup>1</sup>
6	<sup>1</sup> Biology Department, Reed Co	ollege, Portland, OR 97202
7	<sup>2</sup> Biology Department, Univers	ity of Utah, Salt Lake City, UT 84112
8		
9	Corresponding author:	Erik Zornik
10		3203 SE Woodstock Blvd
11		Portland, OR 97202
12		Email: ezornik@reed.edu
13		
14	Number of pages: 27	
15	Number of figures: 7	
16	Number of words: Abstract, 23	31; Introduction, 583; Discussion, 1472
17		
18	Acknowledgements	
19	We thank Charlotte Barkan an	d two anonymous reviewers for helpful feedback on the manuscript. This
20		nal Institutes of Health (NS091977) and start-up funds from Reed College
	•	
21	The authors declare no compe	ing mancial interests.
22		

#### ABSTRACT

23

24

25

26

27

28

29

30

31

32

33

34

35

36

37

38

39

Central patterns generators (CPGs) are neural circuits that drive rhythmic motor output without sensory feedback. Vertebrate CPGs are generally believed to operate in a top-down manner in which premotor interneurons activate motor neurons that in turn drive muscles. In contrast, the frog (Xenopus laevis) vocal CPG contains a functionally unexplored neuronal projection from the motor nucleus to the premotor nucleus, indicating a recurrent pathway that may contribute to rhythm generation. In this study we characterized the function of this bottom-up connection. The X. laevis vocal CPG produces a 50-60 Hz "fast trill" song used by males during courtship. We recorded "fictive vocalizations" in the in vitro CPG from the laryngeal nerve while simultaneously recording premotor activity at the population and singlecell level. We show that transecting the motor-to-premotor projection eliminated the characteristic firing rate of premotor neurons. Silencing motor neurons with the intracellular sodium channel blocker QX-314 also disrupted premotor rhythms, as did blockade of nicotinic synapses in the motor nucleus (the putative location of motor neuron-to-interneuron connections). Electrically stimulating the laryngeal nerve elicited primarily inhibitory post-synaptic potentials in premotor neurons that could be blocked by a nicotinic receptor antagonist. Our results indicate that an inhibitory signal, activated by motor neurons, is required for proper CPG function. To our knowledge, these findings represent the first example of a CPG in which precise premotor rhythms are tuned by motor neuron activity.

40

41

42

43

44

45

46

#### SIGNIFICANCE STATEMENT

Central pattern generators (CPGs) are neural circuits that produce rhythmic behaviors. In vertebrates, motor neurons are not commonly known to contribute to CPG function, with the exception of a few spinal circuits where the functional significance of motor neuron feedback is still poorly understood. The frog hindbrain vocal circuit contains a previously unexplored connection from the motor to premotor region.

Our results indicate that motor neurons activate this bottom-up connection, and blocking this signal

eliminates normal premotor activity. These findings may promote increased awareness of potential involvement of motor neurons in a wider range of CPGs, perhaps clarifying our understanding of network principles underlying motor behaviors in numerous organisms, including humans.

50

51

52

53

54

55

56

57

58

59

60

61

62

63

64

65

66

67

68

69

70

#### INTRODUCTION

Central pattern generators (CPGs) are neural networks that produce rhythmic behaviors such as respiration and courtship song. CPGs produce rhythmic output even when isolated from descending inputs or sensory feedback (Marder and Bucher, 2001; Grillner, 2006). In several invertebrate CPGs, motor neurons are an integral part of the circuit, with extensive functional connections with premotor neurons (Arshavsky et al., 1997; Marder and Bucher, 2007; García-Crescioni and Miller, 2011). In the majority of vertebrate CPGs, motor neurons are thought to be passive output cells (Kiehn, 2006, 2011; Guertin and Steuer, 2009), although growing evidence from spinal circuits is challenging this assumption. In chick and rodent spinal CPGs, motor neurons are known to send excitatory projections to Renshaw cells that in turn influence the activity of motor neurons and other Renshaw cells (Wenner and O'Donovan, 1999; Kiehn and Butt, 2003; Nishimaru et al., 2005, 2006). In the Xenopus tadpole swimming CPG, motor neurons synapse onto each other and onto interneurons in the same circuit, and may contribute to rhythm generation (Perrins and Roberts, 1995a; Roberts et al., 2012, 2014). Studies in both chick embryo (Wenner and O'Donovan, 1999, 2001) and embryonic and neonatal rodent spinal cord (Hanson and Landmesser, 2003; Mentis et al., 2005; Machacek and Hochman, 2006; Bonnot et al., 2009) have found electrophysiological and anatomical evidence that motor neurons can activate premotor pathways in the locomotor CPG. In zebrafish, recent work also showed that motor neurons may influence premotor neuron activity via electrical synapses (Song et al., 2016). Thus, there is preliminary evidence indicating that motor neurons can contribute to locomotor rhythm generation. To our knowledge, however, no previous studies have identified motor neuron involvement in non-spinal vertebrate CPGs.

71	The vocal system of the frog $Xenopus\ laevis$ provides a powerful framework for identifying mechanisms
72	of CPG function in the vertebrate hindbrain (Zornik and Kelley, 2011). The vocal CPG can be activated
73	in vitro, enabling the recording of "fictive vocalizations" from the laryngeal nerve along with intracellular
74	and extracellular recordings of premotor activity. A prominent component of the male courtship call, fast
75	trill, consists of repeating trains of $50-60~\mathrm{Hz}$ sound pulses (Wetzel and Kelley, 1983). Premotor neurons
76	termed "fast trill neurons" (FTNs), have been identified that appear to generate the fast trill rhythm
77	(Zornik and Yamaguchi, 2012).
78	The X. laevis vocal CPG consists of two hindbrain nuclei, the premotor nucleus DTAM (used as a proper
79	noun) in the pons, and the laryngeal motor nucleus (n.) IX-X in the caudal hindbrain (Rhodes et al.,
80	2007). Anatomical evidence has indicated that premotor neurons in DTAM project to n.IX-X (Wetzel et
81	al., 1985; Zornik and Kelley, 2007), and electrophysiological experiments have shown that they can
82	directly activate vocal motor neurons (Zornik and Kelley, 2008). The circuit also possesses a prominent
83	ascending projection from n.IX-X to DTAM (Figure 1; Zornik and Kelley, 2007), but its functional role
84	has not been previously investigated.
85	The goal of this study was to examine the role of this feedback projection. Due to mounting evidence of
86	motor neuron involvement in spinal circuits, we hypothesized that motor neurons may also contribute to
87	the function of CPGs located in the brain. We used a combination of physical transections,
88	pharmacological perturbations, whole-cell patch-clamp recordings, and nerve stimulations in the fictively
89	vocalizing isolated brain preparation to test the hypothesis that the motor-to-premotor projection is
90	activated by vocal motor neurons, and that it is required for generating normal premotor vocal rhythms.
91	Our results support the hypothesis that motor neurons tune vocal patterns by activating ascending
92	interneurons.

# 93 MATERIALS AND METHODS

94 Animals

95 Adult male wild type *Xenopus laevis* frogs (Nasco) (weight,  $43.3 \pm 7.3$  g; length,  $7.1 \pm 0.5$  cm) were group-housed (up to 15 per tank) in recirculating water in PETG aquaria (Aquaneering) and maintained 96 97 on a 12:12 hour light:dark cycle. Protocols were approved by the Reed College Institutional Animal Care 98 and Use Committee. 99 In vitro brain preparation 100 To isolate brains for fictive vocal recordings, animals were anesthetized with subcutaneous injections of 101 0.5 – 0.7 ml of 1.3% tricaine methanesulfonate (MS-222; Sigma), placed on ice for at least five minutes, 102 and decapitated. Brains were extracted in a dish containing ~10°C saline (in mM: 96 NaCl, 20 NaHCO<sub>3</sub>, 103 11 glucose, 10 HEPES, 2 CaCl<sub>2</sub>, 2 KCl, and 0.5 MgCl<sub>2</sub>; at pH 7.8) which was continuously oxygenated 104 with 99% O<sub>2</sub>/1% CO<sub>2</sub>. Isolated brains were pinned in a petri dish lined with silicone elastomer (Sylgard; 105 Dow Corning) containing oxygenated saline. The roots of cranial nerve N.IX-X were cut except for the 106 most caudal root containing all laryngeal motor neuron axons (Simpson et al., 1986) (referred to here as 107 the laryngeal nerve). A dorsal midline cut was made through the center of the cerebellum and optic tectum between the 3<sup>rd</sup> and 4<sup>th</sup> ventricles, dorsal to the ventricle floor. This region was then pinned 108 109 laterally to allow access to the vocal premotor nucleus, DTAM, as previously described (Zornik and 110 Yamaguchi, 2012). After one hour, brains were transferred to a Sylgard-lined petri recording dish 111 continuously perfused with ~22°C oxygenated saline. In some experiments, transverse transections were made just caudal to N.VIII, thus severing the connections between n.IX-X and DTAM. 112 113 Electrophysiology 114 Serotonin (5-HT) bath-applied to isolated brains induces trains of compound action potentials (CAPs) in 115 the laryngeal nerve. These CAP trains represent "fictive" vocalization, as they closely match the activity 116 recorded during calling in intact frogs (Yamaguchi and Kelley, 2000; Rhodes et al., 2007). We measured 117 fictive vocalizations by placing a suction electrode over the cut end of N.IX-X (Figure 2A). In nerve

silencing experiments (described below), cut nerve endings were placed in vaseline wells; to perform

Pharmacological manipulations

119	differential recordings in this configuration, one silver wire electrode was placed inside the well and the
120	other silver wire electrode was placed just outside the well. Simultaneous LFP recordings were obtained
121	via a 0.5 M $\Omega$ tungsten electrode (Microprobes) inserted into DTAM.
122	Nerve recordings and DTAM local field potential (LFP) signals were amplified 1000x (differential
123	amplifier models 1700 and 1800, respectively; A-M Systems) and band-pass filtered (10 Hz $-5\ kHz$ and
124	$0.1-5\ \mathrm{kHz}$ , respectively). All signals were digitized at 10 kHz and recorded with Clampex software
125	(Molecular Devices).
126	Whole-cell recordings were obtained in DTAM at depths of $79-207~\mu m$ below the ventricular surface, as
127	previously described (Zornik and Yamaguchi, 2012). Patch-clamp electrodes (6 – 10 $M\Omega)$ were made
128	from thick-walled borosilicate capillary tubes (1.5 mm outer diameter; 0.86 mm inner diameter), pulled
129	on a Flaming/Brown style microelectrode puller (P-1000; Sutter Instruments). A blind search strategy was
130	used to locate premotor neurons in DTAM: positive pressure was applied to the electrode before
131	advancing vertically into DTAM using a motorized micromanipulator (MC1000e; Siskiyou). Cell
132	searches began after the electrode reached a depth of 50 $\mu m,$ after which the electrode was slowly
133	advanced through the tissue until encountering a rapid and reliable increase in resistance, indicating
134	proximity to a cell. Positive pressure was then released, a gigaohm (G $\Omega$ ) seal obtained, and brief negative
135	suction applied to achieve whole-cell access. Whole-cell recordings were determined to be premotor
136	neurons based on their synchronized activity with 5HT-induced fictive fast trills or LFP waves.
137	For nerve stimulations, brief (100 $\mu s)$ isolated current pulses were generated through the suction electrode
138	on the laryngeal nerve (Model 3800 stimulator, A-M Systems). Currents were increased until a post-
139	synaptic potential (PSP) was observed in the whole-cell recording. Effective current intensities ranged
140	from 200 $\mu A$ – 2 mA. Stimulation trials consisted of 10 single pulses given every 10 seconds. During
141	pharmacological experiments, trials were repeated every 10 minutes.

143	For eliciting fictive song in all experiments, saline superfusion was paused and 500 µl of 5-HT solution
144	was added to the recording bath (60 $\mu M$ final concentration). After 3 – 4 min of recording, superfusion
145	was resumed (>200 ml/hr) for 1 hour to wash out the serotonin.
146	To inactivate motor neurons, the intracellular Na <sup>+</sup> channel blocker QX-314 (200 mM, Sigma) was added
147	to vaseline wells formed around the cut ends of N.IX-X prior to recording premotor whole-cell and LFP
148	activity. QX-314 was applied to the wells immediately following control 5-HT-induced fictive
149	vocalizations, and allowed to diffuse into nerve axons during the 1 hour wash period.
150	During some stimulation experiments (described above), the nicotinic acetylcholine receptor (AChR)
151	blocker tubocurarine (25uM, Tocris) was bath applied while recording from individual premotor neurons.
152	After obtaining stimulation-induced PSPs, tubocurarine was bath-applied and additional stimulations
153	were made 10 minutes later; superfusion was then reinstated for the one-hour drug washout, while
154	stimulations were continually repeated every 10 minutes.
155	To locally block cholinergic synapses in the motor nucleus, we injected tubocurarine into n.IX-X via
156	pressure injection (Picospritzer III; Parker Hannifin). Tubocurarine mixed with in 7.5%
157	tetramethyrhodamine dextran (3000 MW; Thermo Fisher Scientific) was loaded into a thick-walled
158	borosilicate capillary tube (1.5 mm outer diameter; 0.86 mm inner diameter) pulled (P1000, Sutter) and
159	broken to a tip diameter of 20 - 30 $\mu m.$ The pipette was lowered into n.IX-X using a motorized
160	micromanipulator (MC1000e; Siskiyou) to a depth of $800-900~\mu m$ below the dorsal surface. A series of
161	20 ms duration pressure pulses at 20 psi were applied; all brains received between 100 and 200 pulses,
162	until substantial dye was observed in the area. High doses (5 mM or 25 mM, final concentration) were
163	used to compensate for dilution of the small injection volumes. Control experiments were identical except
164	physiological saline replaced tubocurarine in the dye mixture. Only experiments where brains produced at
165	least 5 trills after a $1-2$ hour washout were included in the dataset.
166	Histology

167	Injection sites in antero-medial n.IX-X were confirmed via cryosectioning at 30 $\mu m$ on a Leica cryostat
168	and visualized on an upright wide-field fluorescence microscope (Olympus, model BX60). Sectioning and
169	imaging analysis were performed blind to experimental group.
170	Data analysis
171	Clampfit software (Molecular Devices, Sunnyvale, CA) threshold search was used to quantify
172	instantaneous spike rate for 10 spike bursts per premotor neuron. Instantaneous spike frequencies were
173	calculated as the reciprocal of each spike interval; histograms were generated by calculating the percent
174	of instantaneous spike frequencies at each frequency range (bins = 5 Hz for quantification, 10 Hz for
175	graphical representations).
176	Clampfit threshold search was used to quantify CAP amplitude of nerve recordings for tubocurarine (5
177	mM) injection experiments. The last 10 CAPs in each trill were measured, using $5-10$ trills per
178	experiment.
179	Normal premotor vocal LFP recordings consist of slow waves containing phasic activity at fast trill rates
180	$(50-60\ Hz)$ . LFP waves persist after transection, although phasic activity is lost (Zornik et al., 2010). To
181	quantify premotor neuron population activity, power spectra of LFP waves were compared in intact and
182	experimental brains. Power spectra were calculated from the last 500 ms of each wave for 5 consecutive
183	waves in each brain. In experiments where we also measured motor neuron population activity, power
184	spectrum analysis was performed on nerve activity occurring during the LFP waves. The power spectra
185	were generated in Clampfit and normalized to the peak of their respective pre-treatment controls. Power
186	data for frequencies less than 10 Hz were excluded.
187	For nerve stimulation-induced PSPs, traces from at least 5 stimulations were averaged; peak onset latency
188	was measured as the time of $10\%$ maximum peak amplitude. The PSP amplitude was calculated from the
189	averaged trace as the maximum voltage change relative to the pre-stimulation resting potential.

Statistics

All statistical tests were performed in Prism 7. The Mann-Whitney U test was used for experiments with two independent groups: comparison of the intact versus transected premotor neuron peak firing frequency, comparison of the change in peak frequency for the saline and 5 mM tubocurarine injections, and comparison of the contralateral versus ipsilateral side for premotor neuron PSP amplitude and latency (relative to the stimulated nerve). No statistical tests were performed on the QX-314 FTN data due to small sample size (n=3). The 25 mM tubocurarine injections were omitted from the change in peak frequency analysis due to the lack of a measurable peak. To assess the relative nerve or LFP power at control peak frequencies following pressure injections (saline, 5 mM tubo, and 25 mM tubo), we used the Kruskal-Wallis test (for three independent groups) with Dunn's post-hoc test with correction for multiple comparisons. To assess the effect of tubocurarine on PSP amplitude in premotor neurons during nerve stimulations, we used the Friedman test for repeated measures with Dunn's post-hoc test with correction for multiple comparisons. Data are reported as mean ± standard error of the mean.

### **RESULTS**

#### Normal premotor activity requires motor nucleus feedback

The male advertisement call is a temporally precise series of sound pulses produced at stereotyped rates, resulting from contraction of a single set of laryngeal muscles (Tobias and Kelley, 1987; Yager, 1992). Each sound pulse is generated by synchronous firing of a pool of motor neurons, which produce compound action potentials (CAPs) in the laryngeal nerve (caudal root of N.IX-X) that lead to activation of the laryngeal muscles (Yamaguchi and Kelley, 2000). In response to serotonin (5-HT) application to the intact *in vitro* brain (**Figure 2A**), the predominant fictive vocalization recorded from N.IX-X begins with a relatively slow and variable CAP repetition rate (20 – 40 Hz) followed by a fast trill, a 50 – 60 Hz train of CAPs (**Figure 2B**, **top trace**). This pattern of nerve activity is similar to the CAP trains recorded from the laryngeal nerve of males calling *in vivo* (Yamaguchi and Kelley, 2000). Local field potential

214	(LFP) recordings in DTAM reveal phasic bursts that correspond to each nerve CAP. Throughout fictive
215	calling, there is a slow LFP wave that coincides with the onset and offset of each fast trill (Zornik et al.,
216	2010) (Figure 2B, middle trace).
217	We wished to identify the functional significance of neuronal projections from the vocal motor nucleus
218	(n.IX-X) to the premotor nucleus, DTAM (Figure 1). To do so, we recorded population level LFP and
219	single-cell level (patch-clamp recordings) premotor activity in DTAM before and after physically
220	transecting between the motor and premotor nuclei (Figure 2). It was previously shown that 5-HT-
221	induced fictive vocalizations in the laryngeal nerve are eliminated following transections between DTAM
222	and n.IX-X (Rhodes et al., 2007). 5-HT application continues to induce DTAM LFP waves in transected
223	brains, but phasic 50 – 60 Hz activity is lost (Zornik et al., 2010) ( <b>Figure 2D, top trace</b> ). Power spectra
224	of LFP activity between 10 and 85 Hz clearly demonstrate the dramatic effect of transection; LFP
225	recordings in intact brains show a strong peak between 50 and 60 Hz, but this frequency band is
226	completely eliminated following transection (Figure 2E; $n = 5$ brains). These results suggest that
227	synchronous premotor activity is eliminated by disrupting the motor-to-premotor projection.
228	Individual neurons in the premotor nucleus DTAM show similar activity patterns to LFP activity (Zornik
229	and Yamaguchi, 2012). "Fast trill neurons" (FTNs) produce a long-lasting depolarization throughout each
230	fictive fast trill and LFP wave, and generate spikes phase-locked to each CAP (Figure 2B, bottom trace)
231	with each spike followed by an IPSP (Figure 2B, inset, bottom trace, arrows). In transected brains,
232	FTNs continue to generate long lasting depolarizations in response to 5-HT application. These
233	depolarizations occur during each LFP wave, as in the intact brain, however, the FTN spikes are no longe
234	generated at primarily fast trill frequencies during these depolarizations (Figure 2D, bottom trace).
235	To quantify the differences in FTN firing patterns, we generated histograms of instantaneous spike
236	frequencies (bin width: 5 Hz) and scatterplots of spike frequencies over trill duration. In intact brains,
237	instantaneous firing rates are clustered around a clear peak in the range associated with fictive fast trills.

238	Peak spike rates for individual FTNs ranged between 50 and 65 Hz ( $55.8 \pm 2.2$ Hz; <b>Figure 2F</b> ; n = 6
239	cells in 6 brains). A smaller peak at $\sim$ 30 Hz is also prominent due to occasional spike failures during the
240	$\sim$ 60 Hz fast trill. In the intact brain, the majority of FTN spikes occur at fast trill rates (50 – 60 Hz;
241	Figure 2G). Scatterplots of individual FTNs reveal that most cells increase their spike rate at the
242	beginning of each trill before attaining characteristic fast trill rates (Figure 3A-C). In some cells, higher
243	frequency spike rates occur due to the presence of doublet and triplet spikes associated with each nerve
244	CAP (Fig 3C; Zornik and Yamaguchi, 2012).
245	In contrast, FTN spike rates in transected brains tended to be more variable both within and between
246	neurons compared to recordings in intact brains. Frequency peaks ranged from 45 – 170 Hz. Overall, the
247	average FTN peak spike frequency was significantly faster compared to intact brains (Figure 2F; peak =
248	$96.7 \pm 13.5$ Hz; n = 9 cells in 9 brains; $U = 6.5$ , $P = 0.0132$ ). Spikes were not only faster, but also
249	occurred at a broader range of rates in transected brains (Figure 2G). Some individual neurons fired
250	within a relatively narrow frequency band, albeit at higher than normal rates (Figure 3D). Most neurons,
251	however, exhibited a broader firing rate distribution, typically much faster than controls (Figure 3E,F).
252	Scatterplots show that in transected brains, FTN spike rates often increase throughout each burst, attaining
253	faster and broader ranges of spike rates than controls (Figure 3E,F). These findings, together with the
254	results of our population-level analyses, suggest that the motor-to-premotor projection is essential for
255	tuning the premotor fast trill rhythm.
256	Effect of silencing motor neurons
257	We wished to test whether motor neurons themselves might be responsible for activating the motor-to-
258	premotor projection. To test whether n.IX-X feedback to DTAM depends on motor neuron activity, we
259	silenced vocal motor neurons in the intact brain by backfilling the laryngeal nerve with the intracellular
260	sodium channel blocker QX-314 (Figure 4A). LFP and whole-cell recordings during these experiments

were similar to those observed in transection experiments (Figure 4B). Slow LFP waves in DTAM were

263

264

265

266

267

268

269

270

271

272

273

274

275

276

277

278

279

280

281

282

283

284

285

still induced by 5-HT application, but the 50-60 Hz phasic patterns were absent, as evidenced by the dramatic loss of power in that frequency range (Figure 4C; n = 5 brains). Corresponding FTN activity was also faster and more variable than controls, with peak rates ranging between 70 and 90 Hz (Figure **4D**; n = 3 cells in 3 brains; no statistical test was performed due to the small sample size). These results indicate that (1) transection results can be explained by the loss of inputs from motor neurons and (2) motor neurons activate the motor-to-premotor feedback signal necessary for appropriate premotor tuning. Blocking cholinergic signaling in n.IX-X disrupts premotor activity Previous anatomical experiments revealed a motor-to-premotor projection that arises from a population of interneurons in antero-medial n.IX-X that project to DTAM (Zornik and Kelley, 2007). We hypothesized that motor neurons may act on the premotor circuit by exciting these intervening interneurons in n.IX-X. To test this, we used the nicotinic acetylcholine receptor (nAChR) blocker tubocurarine, which reversibly antagonizes nAChRs and therefore blocks synaptic transmission of motor neurons (Usiak and Landmesser, 1999). To avoid affecting other brain regions, we locally applied tubocurarine (or a saline control) into antero-medial n.IX-X via pressure injection (Figure 5A). In control experiments, brains produced largely normal fictive vocalizations following saline injection, whereas low-dose (5 mM) and high-dose (25 mM) tubocurarine injections produced significant or complete disruption of CPG function, respectively (Figure 5B). In 4 of 9 brains with low-dose injections, fictive fast trills were blocked, although most of these (3 of 4 brains) did produce slow CAP trains without LFP waves. In the other 5 cases, fictive fast trills were still produced (Figure 5B), although CAP amplitude was reduced to  $43 \pm 4\%$ of the pre-injection control. In contrast, no fictive calling was produced following high-dose injections,

although LFP waves (as seen in transected and motor neuron-silenced brains) were still induced by 5-HT.

Unlike motor neuron silencing by QX-314, the laryngeal nerve was still active following tubocurarine

injection experiments. Therefore, we were able to determine the effect of each treatment on nerve power

spectra following drug injection and 5-HT application. Following saline control experiments, there was

286	no clear change in the most prominent frequencies recorded in the nerve relative to pre-injection controls
287	(Figure 5C; $n = 6$ brains). In response to 5 mM tubocurarine, there was a slight leftward shift in the most
288	prevalent frequencies (Figure 5D; $n = 5$ brains), whereas 25 mM tubocurarine completely abolished fast
289	trill frequencies ( <b>Figure 5E</b> ; $n = 5$ brains). Thus, local blockade of nAChRs in n.IX-X eliminates vocal
290	motor production. Statistical analyses of nerve recordings revealed that, compared to saline injection, a
291	high dose of tubocurarine significantly reduced the power relative to the pre-injection control peak
292	frequencies ( <b>Figure 5I</b> ; Saline: $0.56 \pm 0.24~\mu\text{V}^2~\text{Hz}^{\text{-1}};~5\text{mM}:~0.088 \pm 0.031~\mu\text{V}^2~\text{Hz}^{\text{-1}};~25\text{mM}:~0.0014 \pm 0.0014$
293	$0.0004~\mu\text{V}^2~\text{Hz}^{-1};~\textit{H}=12.51,~\textit{P}=0.0012).$ In addition to qualitative differences in nerve activity, 5 mM
294	tubocurarine injections significantly decreased the peak nerve frequencies compared with saline injections
295	( <b>Figure 5J</b> ; Saline: $-0.81 \pm 1.21$ Hz; 5mM: $-9.28 \pm 2.49$ Hz; $U = 2.5$ , $P = 0.0216$ ). Following 25 mM
296	tubocurarine injections, there was no discernable peak in the fast trill frequency range (Figure 5E), so
297	these data were not included in the analysis of the change in peak frequency.
298	Changes in LFP power spectra mirrored those of nerve spectra. Saline injection had no obvious effect on
299	LFP frequencies ( <b>Figure 5F</b> ; n = 6 brains), 5 mM tubocurarine injections caused a shift to a lower band
300	of frequencies ( <b>Figure 5G</b> ; n = 4 brains), and 25 mM tubocurarine eliminated all fast trill frequencies
301	(Figure 5H; n = 4 brains). The relative power at the peak LFP frequency was significantly lower
302	following the 25 mM tubocurarine injections (Figure 5K; Saline: $0.61 \pm 0.10~\mu\text{V}^2~\text{Hz}^{-1}; 5~\text{mM}: 0.14 \pm 0.10~\mu\text{V}^2$
303	$0.049~\mu\text{V}^2~\text{Hz}^{-1};~25~\text{mM}:~0.011\pm0.0075~\mu\text{V}^2~\text{Hz}^{-1};~\textit{H}=11.02,~\textit{P}=0.0035).$ As with nerve recordings,
304	there was a significant decrease in peak frequency relative to control following 25 mM tubocurarine
305	injection ( <b>Figure 5L</b> ; Saline: $0.00 \pm 1.78$ Hz; 5 mM: $-8.55 \pm 1.22$ Hz; $U = 0$ , $P = 0.0048$ ). Taken together
306	these results show local blockade of nAChRs in n.IX-X eliminates both laryngeal nerve output and
307	premotor rhythm generation.

Motor-to-premotor pathway: nerve stimulations

Tubocurarine injections into n.IX-X (Figure 5) had a similar effect on premotor activity as brain
transections (between n.IX-X and DTAM; Figure 2) and motor neuron silencing (Figure 4), supporting
the hypothesis that the motor-to-premotor feedback interneurons may be activated by cholinergic motor
neuron inputs. If this hypothesis is correct, then there must be an indirect connection (at least two
synapses) between n.IX-X motor neurons and premotor neurons in DTAM. To test this prediction, we
stimulated N.IX-X while recording individual fast trill neurons (Figure 6A). 12 of 15 FTNs showed an
observable response to stimulations, with most of these displaying a relatively short latency inhibitory
post-synaptic potential (IPSP; 11 of 12 cases), with onset times ranging from 7.8 to 20.8 ms (Figure 6B-
C; $12.9 \pm 1.15$ ms). The average PSP amplitude varied between -1.1 mV to -8.0 mV (Figure 6D; mean $\pm$
SEM: $3.52 \pm 0.63$ mV). In 1 case we instead observed a relatively short latency (22 ms) excitatory post-
synaptic potential (EPSP) with an average amplitude of 6.6 mV (not shown). The onset of IPSPs elicited
by contralateral stimulations were significantly delayed (15.7 $\pm$ 1.6 ms, n = 5 cells in 5 brains) compared
to those elicited by ipsilateral stimulations (10.5 $\pm$ 0.9 ms; n = 6 cells in 6 brains; $U = 3$ , $P = 0.0303$ , n = 5
cells in 5 brains; <b>Figure 6C</b> ). The amplitude of IPSPs induced by contralateral stimulations (-3.8 $\pm$ 1.0
mV) were not significantly different from those arising from ipsilateral stimulations (-3.3 $\pm$ 0.8 mV; $U =$
11.5, $P = 0.5714$ ; <b>Figure 6D</b> ).
Results of tubocurarine injections into n.IX-X support the prediction that the putative link between motor
neurons and DTAM premotor neurons involves nAChRs. To test this, we bath-applied tubocurarine (25
$\mu M)$ during nerve stimulation to block putative motor neuron inputs onto feedback projection
interneurons. Drug application rapidly and reversibly blocked PSPs in 5 of 5 cells (from 5 separate brains)
( <b>Figure 6E-F</b> ; Friedman test, $P = 0.0133$ ). Together, these results reveal the existence of a connection
between n.IX-X motor neurons and premotor vocal neurons, supporting the notion that motor neuron
activity tunes rhythmic premotor activity.

DISCUSSION

333	The goal of this study was to identify the function of an ascending motor-to-premotor projection in the $X$
334	laevis vocal CPG. Our results indicate that this projection provides a feedback signal that tunes and
335	synchronizes the activity of fast trill neurons, "FTNs", in the premotor nucleus, DTAM. This feedback
336	signal is activated by motor neurons via cholinergic input onto interneurons that project to DTAM. Thus,
337	vocal CPG function is regulated by motor neurons.
338	Motor nucleus feedback tunes and synchronizes premotor spiking
339	Our results provide strong evidence that the feedback projection tunes premotor activity underlying fast
340	trill production. In transected brains FTNs depolarize and spike during LFP waves, but spike rates were
341	faster than in intact brains. LFP power spectra in transected brains revealed a complete loss of the $50-60$
342	Hz phasic activity, indicating the loss of synchronous premotor spiking. Therefore, the feedback
343	projection appears to serve two functions: it slows FTN spiking and promotes spike synchrony.
344	Vocal rhythms and premotor synchrony require motor neuron input
345	Back-filling laryngeal nerve axons with an intracellular sodium channel blocker, QX-314, recapitulated
346	the effect of transections; 5-HT induced DTAM LFP waves that lacked the fast trill rhythms, and FTNs
347	produced spikes at faster and broader rates than in controls. Because studies have shown that QX-314
348	does not cross gap junctions (Mann-Metzer and Yarom, 1999; Curti and Pereda, 2004), the treatment is
349	most likely due to silencing of motor neurons themselves, not indirectly silencing electrically coupled
350	interneurons. We therefore hypothesized that axon collaterals from motor neurons activate interneurons
351	that project to DTAM.
352	In support of this hypothesis, injecting a nAChR antagonist into antero-medial n.IX-X (where motor-to-
353	premotor projection neurons are found; Zornik and Kelley, 2007) also disrupted premotor rhythms, as
354	determined by a loss of phasic activity in LFP waves. Also in support of our hypothesis, we identified a

relatively short-latency (7.8 – 20.8 ms), primarily inhibitory, input to FTNs that was activated by

356	laryngeal nerve stimulation and required nicotinic signaling. Together, we provide multiple lines of
357	evidence supporting the hypothesis that motor neurons may indirectly modulate premotor neuron firing.
358	One caveat to the interpretation above is that the laryngeal nerve innervates two distinct muscles: the
359	laryngeal dilators, and the glottal muscles (located in the anterior larynx) (Zornik and Kelley, 2007).
360	Thus, it is possible that inhibitory inputs to FTNs following nerve stimulation arise from glottal motor
361	neuron activation. This scenario is unlikely, however, given the results of motor neuron silencing.
362	Because we know that glottal motor neurons are not active during vocalization (Rhodes et al., 2007;
363	Zornik and Kelley, 2008), it is implausible that inactivation of glottal motor neurons would affect the
364	vocal CPG. We conclude the most likely scenario is that laryngeal motor neurons activate feedback
365	neurons that ultimately inhibit premotor FTNs.
366	Proposed model for feedback-dependent premotor rhythm generation
367	We propose a motor neuron-dependent model of the <i>X. laevis</i> vocal CPG ( <b>Figure 7A</b> ). Because DTAM
368	neurons monosynaptically activate motor neurons (Zornik and Kelley, 2008), and FTNs project to n.IX-
369	X, we predict FTNs directly activate laryngeal motor neurons, which induce laryngeal muscle contraction
370	and sound pulses. At the same time, axon collaterals from motor neurons provide an excitatory,
371	cholinergic signal onto n.IX-X interneurons. These neurons ultimately provide inhibitory feedback inputs
372	to FTNs (directly or via intervening inhibitory interneurons). This model is supported by current and
373	previous findings that FTNs receive inhibitory inputs shortly after each nerve CAP (Fig. 2B; Zornik and
374	Yamaguchi, 2012). When the feedback signal is eliminated (via transection or motor neuron silencing),
375	IPSPs are no longer apparent (Fig. 2D, 7C), leading to an increased spike rate. Therefore, FTN synchrony
376	is maintained in the intact circuit through cycle-by-cycle inhibition allowing synchronous firing upon
377	post-inhibitory rebound (Fig. 7D); in the absence of this entraining signal, FTN spikes become faster and
378	desynchronized (Fig. 7E).

380

381

382

383

384

385

386

387

388

389

390

391

392

393

394

395

396

397

398

399

400

401

402

While our model requires rapid (~5 ms) feedback inhibition, the nerve stimulation-induced IPSPs observed in FTNs ranged from  $\sim 7-20$  ms. A possible explanation for this discrepancy is that feedback interneurons are likely in a hyperpolarized state during nerve-stimulation experiments (when the vocal CPG is inactive). Although nerve stimulation is able to induce a spike in the feedback interneuron in these experiments, the spike onset time of these neurons is likely to be much longer than it would be in the active circuit. In the activated neurons, the synaptic delay is likely shorter due to depolarization (bringing the cell closer to spike threshold), and possibly due to a decrease in time constant of the membrane (caused by the opening of voltage-gated channels). An alternative possibility is that the motor neurondependent feedback inhibition leads to a slow, tonic inhibition that prevents excessive depolarization of FTNs, thus favoring the production of spikes at fast trill rates. Given that phasic IPSPs are eliminated by disrupting the feedback signal, however, we believe the hypothesis that motor neurons drive cycle-bycycle feedback inhibition is the most likely mechanism for tuning FTN firing rate. We measured nerve stimulation-induced IPSPs in FTNs both ipsilateral and contralateral to the stimulated nerve. IPSP amplitudes did not vary between ipsilateral and contralateral inputs, suggesting a potential role for the feedback pathway in maintaining bilateral synchrony of motor output, a requirement for sound production (Yager, 1992). We did find a difference in IPSP latency, however, with IPSP latency in ipsilateral FTNs being shorter than to contralateral FTNs. As discussed above, it is possible that feedback latency in the active CPG is much shorter, and the actual difference in latencies between ipsilateral and contralateral feedback signals may be negligible during CPG production of fast trill. Future characterization of the synaptic delay between motor neurons and feedback interneurons will be required to resolve this question. Role of motor neurons in vertebrate motor circuits Invertebrate CPGs have been studied in detail in a range of species including crustaceans (Marder and

Bucher, 2007), mollusks (Wentzell et al., 2009), and leech (Kristan et al., 2005; Friesen and Kristan,

404

405

406

407

408

409

410

411

412

413

414

415

416

417

418

419

420

421

422

423

424

425

426

427

2007). In some cases motor neurons participate in the rhythm generating circuit (Marder and Bucher, 2007). In vertebrates, there is far less evidence of motor neuron involvement in CPG function. While connections between motor neurons, both via chemical and electrical synapses, are known to promote network synchrony (Perrins and Roberts, 1995b; Zhang et al., 2009; Chagnaud et al., 2012), there is sparse evidence that motor neurons are playing an active role in regulating CPG activity. One cell type known to receive input from motor neurons is mammalian Renshaw cells, which form a recurrent feedback loop with motor neurons (Bhumbra et al., 2014). Other evidence for motor neuron feedback in mammals comes from embryonic and neonatal rodent spinal cord studies. In embryonic mouse spinal cord, anatomical evidence revealed motor neuron projections to interneuron-containing regions, and motor neurons appeared capable of initiating spontaneous rhythmic bursting, mediated by excitatory glycinergic and GABAergic interneurons (Hanson and Landmesser, 2003). In mice and rats, stimulating ventral locomotor nerve roots in the disinhibited spinal cord elicits locomotor-like bursting (Machacek and Hochman, 2006; Bonnot et al., 2009; O'Donovan et al., 2010), suggesting the presence of motor neuron collaterals onto interneurons other than Renshaw cells. In the *Xenopus* tadpole swimming CPG, blocking presumptive motor neuron synapses disrupts normal rhythms in premotor interneurons (Perrins and Roberts, 1995a). In the chick, putative avian Renshaw cell homologs, R-interneurons, appear capable of inducing locomotor circuit activity; spontaneous bouts of activity seem to be driven or enhanced by motor neurons, as blocking cholinergic receptors reduces this phenomenon (Wenner and O'Donovan, 1999, 2001). These results indicate that, at least during embryonic stages, R-interneurons project to CPG neurons in the locomotor circuit (activation is likely due to the fact that R-interneurons are excitatory during embryonic development). If these projections persist in adulthood, it would provide a pathway for motor neurons to influence CPG function, albeit via inhibition, as R-interneurons are inhibitory in adults. Because the above studies were performed in embryonic and neonatal animals, it is not clear whether these connections via chemical synapses persist in adult vertebrate spinal circuits. However, recent work

in the juvenile and adult zebrafish swimming CPG showed that motor neurons can influence premotor
activity via gap junctions rather than chemical transmission (Song et al., 2016). This finding provides an
example of motor neuron involvement later in development, and extends the number of studies indicating
an active role for motor neurons in locomotor CPGs.
To our knowledge, the findings in this study represent the first evidence that motor neurons can regulate a
hindbrain CPG. This raises the intriguing possibility that motor neuron involvement in CPG function is
more common than generally assumed, and therefore warrants examination in other non-spinal CPGs.
Such investigations may find that canonical top-down models of vertebrate motor circuits, in which motor
neurons act as relays between CPG neurons and muscles, are incomplete. Instead, vertebrate circuits may
more closely resemble invertebrate CPGs, with motor neurons serving as critical components of CPGs.
REFERENCES
Arshavsky YI, Deliagina TG, Orlovsky GN (1997) Pattern generation. Curr Opin Neurobiol 7:781–789.
Bhumbra GS, Bannatyne XBA, Watanabe M, Todd XAJ, Maxwell DJ, Beato XM (2014) The Recurrent
Case for the Renshaw Cell. 34:12919–12932.
Bonnot A, Chub N, Pujala A, O'Donovan MJ (2009) Excitatory actions of ventral root stimulation during
network activity generated by the disinhibited neonatal mouse spinal cord. J Neurophysiol
101:2995–3011.
Chagnaud BP, Zee MC, Baker R, Bass AH (2012) Innovations in motoneuron synchrony drive rapid
temporal modulations in vertebrate acoustic signaling. J Neurophysiol 107:3528–3542.
Curti S, Pereda AE (2004) Voltage-Dependent Enhancement of Electrical Coupling by a Subthreshold
Sodium Current. J Neurosci 24:3999–4010.

450	Friesen WO, Kristan WB (2007) Leech locomotion: swimming, crawling, and decisions. Curr Opin
451	Neurobiol 17:704–711.
452	García-Crescioni K, Miller MW (2011) Revisiting the reticulum: feedforward and feedback contribution
453	to motor program parameters in the crab cardiac ganglion microcircuit. J Neurophysiol 106:2065-
454	2077.
455	Grillner S (2006) Biological Pattern Generation: The Cellular and Computational Logic of Networks in
456	Motion. Neuron 52:751–766.
457	Guertin P a., Steuer I (2009) Key central pattern generators of the spinal cord. J Neurosci Res 87:2399-
458	2405.
459	Hanson MG, Landmesser LT (2003) Characterization of the circuits that generate spontaneous episodes
460	of activity in the early embryonic mouse spinal cord. J Neurosci 23:587-600.
461	Kiehn O (2006) Locomotor circuits in the mammalian spinal cord. Annu Rev Neurosci 29:279–306.
462	Kiehn O (2011) Development and functional organization of spinal locomotor circuits. Curr Opin
463	Neurobiol 21:100–109.
464	Kiehn O, Butt SJB (2003) Physiological, anatomical and genetic identification of CPG neurons in the
465	developing mammalian spinal cord. Prog Neurobiol 70:347–361.
466	Kristan WB, Calabrese RL, Friesen WO (2005) Neuronal control of leech behavior. Prog Neurobiol
467	76:279–327.
468	Machacek DW, Hochman S (2006) Noradrenaline unmasks novel self-reinforcing motor circuits within
469	the mammalian spinal cord. J Neurosci 26:5920–5928.
470	Mann-Metzer P, Yarom Y (1999) Electrotonic coupling interacts with intrinsic properties to generate
<b>4</b> 71	synchronized activity in cerebellar networks of inhibitory interneurons. J Neurosci 19:3298–3306

472	Marder E, Bucher D (2001) Central pattern generators and the control of rhythmic movements. Curr Biol
473	11:R986-96.
474	Marder E, Bucher D (2007) Understanding circuit dynamics using the stomatogastric nervous system of
475	lobsters and crabs. Annu Rev Physiol 69:291–316.
476	Mentis GZ, Alvarez FJ, Bonnot A, Richards DS, Gonzalez-Forero D, Zerda R, O'Donovan MJ (2005)
477	Noncholinergic excitatory actions of motoneurons in the neonatal mammalian spinal cord. Proc Nat
478	Acad Sci U S A 102:7344–7349.
479	Nishimaru H, Restrepo CE, Kiehn O (2006) Activity of Renshaw cells during locomotor-like rhythmic
480	activity in the isolated spinal cord of neonatal mice. J Neurosci 26:5320-5328.
481	Nishimaru H, Restrepo CE, Ryge J, Yanagawa Y, Kiehn O (2005) Mammalian motor neurons corelease
482	glutamate and acetylcholine at central synapses. Proc Natl Acad Sci U S A 102:5245–5249.
483	O'Donovan MJ, Bonnot A, Mentis GZ, Chub N, Pujala A, Alvarez FJ (2010) Mechanisms of excitation
484	of spinal networks by stimulation of the ventral roots. Ann N Y Acad Sci 1198:63-71.
485	Perrins R, Roberts A (1995a) Cholinergic contribution to excitation in a spinal locomotor central pattern
486	generator in Xenopus embryos. J Neurophysiol 73:1013–1019.
487	Perrins R, Roberts a (1995b) Cholinergic and electrical synapses between synergistic spinal
488	motoneurones in the Xenopus laevis embryo. J Physiol 485 ( Pt 1:135-144.
489	Rhodes HJ, Yu HJ, Yamaguchi A (2007) Xenopus vocalizations are controlled by a sexually
490	differentiated hindbrain central pattern generator. J Neurosci 27:1485–1497.
491	Roberts A, Conte D, Hull M, Merrison-Hort R, al Azad AK, Buhl E, Borisyuk R, Soffe SR (2014) Can
492	simple rules control development of a pioneer vertebrate neuronal network generating behavior? J
493	Neurosci 34:608–621.

494	Roberts A, Li W-C, Soffe SR (2012) A functional scaffold of CNS neurons for the vertebrates: the
495	developing Xenopus laevis spinal cord. Dev Neurobiol 72:575–584.
496	Simpson HB, Tobias ML, Kelley DB (1986) Origin and identification of fibers in the cranial nerve IX-X
497	complex of Xenopus laevis: Lucifer Yellow backfills in vitro. J Comp Neurol 244:430-444.
498	Song J, Ampatzis K, Björnfors ER, El Manira A (2016) Motor neurons control locomotor circuit function
499	retrogradely via gap junctions. Nature 529:1–5.
500	Tobias ML, Kelley DB (1987) Vocalizations by a sexually dimorphic isolated larynx: peripheral
501	constraints on behavioral expression. J Neurosci 7:3191–3197.
502	Usiak MF, Landmesser LT (1999) Neuromuscular activity blockade induced by muscimol and d-
503	tubocurarine differentially affects the survival of embryonic chick motoneurons. J Neurosci
504	19:7925–7939.
505	Wenner P, O'Donovan MJ (1999) Identification of an interneuronal population that mediates recurrent
506	inhibition of motoneurons in the developing chick spinal cord. J Neurosci 19:7557–7567.
507	Wenner P, O'Donovan MJ (2001) Mechanisms that initiate spontaneous network activity in the
508	developing chick spinal cord. J Neurophysiol 86:1481–1498.
509	Wentzell MM, Martínez-Rubio C, Miller MW, Murphy a. D (2009) Comparative neurobiology of
510	feeding in the opisthobranch sea slug, Aplysia, and the pulmonate snail, Helisoma: evolutionary
511	considerations. Brain Behav Evol 74:219–230.
512	Wetzel DM, Haerter UL, Kelley DB (1985) A proposed neural pathway for vocalization in South African
513	clawed frogs, Xenopus laevis. J Comp Physiol A 157:749–761.
514	Wetzel DM, Kelley DB (1983) Androgen and gonadotropin effects on male mate calls in South African
515	clawed frogs, Xenopus laevis. Horm Behav 17:388–404.

J

516	Yager DD (1992) A unique sound production mechanism in the pipid anuran <i>Xenopus borealis</i> . Zool J
517	Linn Soc 104:351–375.
518	Yamaguchi A, Kelley DB (2000) Generating sexually differentiated vocal patterns: laryngeal nerve and
519	EMG recordings from vocalizing male and female african clawed frogs (Xenopus laevis). J
520	Neurosci 20:1559–1567.
521	Zhang H-Y, Li W-C, Heitler WJ, Sillar KT (2009) Electrical coupling synchronises spinal motoneuron
522	activity during swimming in hatchling Xenopus tadpoles. J Physiol 587:4455–4466.
523	Zornik E, Katzen AW, Rhodes HJ, Yamaguchi A (2010) NMDAR-dependent control of call duration is
524	Xenopus laevis. J Neurophysiol 103:3501–3515.
525	Zornik E, Kelley DB (2007) Breathing and calling: neuronal networks in the Xenopus laevis hindbrain.
526	Comp Neurol 501:303–315.
527	Zornik E, Kelley DB (2008) Regulation of respiratory and vocal motor pools in the isolated brain of
528	Xenopus laevis. J Neurosci 28:612–621.
529	Zornik E, Kelley DB (2011) A neuroendocrine basis for the hierarchical control of frog courtship
530	vocalizations. Front Neuroendocrinol 32:353–366.
531	Zornik E, Yamaguchi A (2012) Coding rate and duration of vocalizations of the frog, Xenopus laevis.
532	Neurosci 32:12102–12114.
533	
534	

Figure	legends
--------	---------

Figure 1. The *X. laevis* adult vocal CPG provides a system for detailed study of a rhythmic motor circuit.

Premotor fast trill neurons (FTN) in DTAM project to vocal motor neurons (MN) in the laryngeal motor nucleus (n.IX-X), which activate laryngeal muscles to produce vocalizations. An interneuron (IN) population projects from motor to premotor nuclei via an uncharacterized synapse (indicated by "?").

540

541

542

543

544

545

546

547

548

549

550

551

552

553

554

555

556

557

558

559

535

536

537

538

539

Figure 2. Normal premotor rhythms require motor nucleus input. (A) Dorsal view of the intact adult X. laevis brain showing the vocal motor nucleus (n.IX-X; red oval) and premotor region (DTAM; blue triangle). Suction electrodes record fictive vocalization from the laryngeal nerve (N.IX-X). Premotor neurons in DTAM are recorded at the population level with a local field potential (LFP) electrode, and individually via a patch-clamp electrode. (B) 5HT-induced fictive vocalizations in the intact brain: the laryngeal nerve (top trace) produces "fast trills" consisting of 50-60 Hz trains of compound action potentials (CAPs). Nerve CAPs coincide with activity in DTAM LFP (middle trace) and patch-clamp (bottom trace) recordings. Red box indicates area of expanded traces; note the presence of IPSPs following each spike (arrows). (C) In order to identify the role of the motor nucleus in tuning premotor rhythms, we transected the brain between n.IX-X and DTAM (dotted line) before recording premotor neuron activity. (D) After transection, 5HT continued to induce premotor activity in DTAM: LFP waves (top trace) persist in transected brains, however, these lack the normal 50 – 60 Hz phasic activity seen in intact brains. Wholecell recordings of premotor fast trill neurons (FTNs; bottom trace) continue to exhibit long-lasting depolarizations during LFP waves, but show altered spike patterns. Red box indicates area of expanded traces. (E) Power spectra of LFP (2.5 Hz bins): intact premotor 50 – 60 Hz rhythms are lost following transection (n = 5 brains). Values are mean  $\pm$  SEM. (F) Mean FTN spike frequency distributions for all intact and transected FTNs (n = 6, 9 cells, respectively, from separate brains). FTN spike rates on average are faster in transected brains. Values are mean ± SEM. (G) Scatterplot of instantaneous FTN spike rates during fast trills (intact) or LFP waves (transected). In intact brains, FTNs tend to spike primarily at fast trill rates; in transected brains, FTN spike rates are faster and more variable. Time zero represents the time of the first spike in each burst. Values are mean ± SEM for all graphs.

560

Figure 3. Spike rate variability within and across individual premotor neurons in intact versus transected brains. (A - C) Scatterplots of spike frequency versus time for three individual premotor FTNs in intact control brains (above) with corresponding spike rate histograms (below). Spike rates increase at the beginning of each trill, with the majority of spikes occurring in the fast trill range of 50 - 60 Hz. Some cells (as in C) also exhibit a higher band of spike rates due to doublet or triplet spikes occurring with some nerve CAPs. Other cells have sporadic low spike rates due to spike failures (as in B). Corresponding spike rate histograms show a major narrow peak in the range of fast trill rates. (D - F) Scatterplots of spike frequency versus time for three individual premotor FTNs recorded in transected brains (above) with corresponding spike rate histograms (below). The majority of FTN spikes in transected brains are produced at rates much faster than the normal range. Some cells maintain a fairly narrow band of spike frequencies (as in D) albeit at higher than normal rates; other cells initially spike near fast trill rates, but then accelerate to faster and broader frequency bands (E and F). Corresponding spike rate histograms show peaks that are faster and broader than those seen in recordings from intact brains.

Figure 4. Silencing motor neurons disrupts premotor rhythms. (A) Laryngeal nerve activity was silenced with the intracellular Na<sup>+</sup> channel blocker QX-314 prior to recording from premotor neurons in DTAM. Circles around nerves indicate vaseline wells that were filled with the drug. (B) Nerve activity is silenced by QX-314 (top trace), but 5HT continues to induce activity in DTAM; LFP waves (middle trace) and long-lasting depolarizations in FTNs (bottom trace) persist, however, these lack the normal fast trill rhythms present in control brains. Red box indicates area of expanded traces. (C) Power spectra of LFP: pre-drug 50 - 60 Hz rhythms are lost following motor neuron silencing by QX-314 (n = 5 brains). Values are mean  $\pm$  SEM. (D) Spike rate histograms for three FTNs show spike rates are faster and more variable in QX-314-treated brains (10 Hz bins; n = 3 cells from separate brains). (E) Mean FTN spike rate distributions for all control and QX-314 FTNs (n = 6, 3 cells, respectively, from separate brains; no statistical tests were performed due to small sample size). Control FTNs same as in Figure 2F. Values are mean  $\pm$  SEM.

Figure 5. Blocking nicotinic ACh receptors (nAChRs) in the motor nucleus disrupts premotor activity. (A)

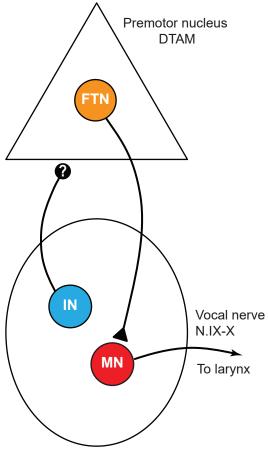
The nAChR blocker tubocurarine or saline was pressure injected bilaterally into n.IX-X while recording the laryngeal nerve and DTAM LFP (injection site shown as pink circles). (B) Simultaneous nerve and LFP recordings

for saline controls, 5 mM tubocurarine, and 25 mM tubocurarine pre-injection (top), immediately following injection (middle), and after washout (bottom). Saline controls produced normal fictive song and DTAM activity, but tubocurarine disrupted CPG function in a dose-dependent manner. (C-E) Power spectra of nerve recordings for saline (C), 5mM tubocurarine (D), and 25mM tubocurarine (E) injections (n = 6,5,5 brains). (F-H) Power spectrum of LFP for saline (F), 5mM tubocurarine (G), and 25mM tubocurarine (H) injections (n = 6,4,4 brains). Values are mean  $\pm$  SEM for all graphs. (I) Effect of tubocurarine injections on nerve power at control peak frequencies relative to saline controls (n = 6,5,5 brains; \*P = 0.0012). (J) Nerve power spectra show a decrease in peak frequency after 5 mM tubocurarine injection compared to saline controls (n = 5,6 brains;). (K) Effect of tubocurarine injections on LFP power at control peak frequencies relative to saline controls (n = 6,4,4 brains; \*P = 0.0035). (L) LFP power spectra show a decrease in peak frequency after 5 mM tubocurarine injections compared to saline controls (n = 4,6 brains; \*P = 0.0048). Each box plot shows individual data points, median, min, max, and interquartile range.

Figure 6. Nerve stimulation induces post-synaptic potentials in premotor FTNs. (A) The laryngeal nerve was electrically stimulated while recording individual premotor neurons in DTAM. (B) Example of a nerve stimulation induced IPSP in a premotor FTN, with 5 example sweeps shown in gray, and an averaged trace in black. (C) Onset latency of IPSPs elicited in FTNs were short latency in ipsilateral and contralateral DTAM (relative to the nerve stimulation electrode; n = 6.5 cells in separate brains; P = 0.03). Each data point represents the value from a single FTN. (D) IPSP amplitudes elicited in FTNs were similar in ipsilateral and contralateral DTAM (P = 0.57). (E) Example traces of nerve stimulations combined with application of the nAChR blocker tubocurarine: no PSPs are observed following application of the drug, but PSPs return following washout. (F) Application of the nAChR blocker tubocurarine completely and reversibly blocks the PSP in all cases, with near-normal return to baseline amplitude after washout (n = 5 cells from separate brains; P = 0.013).

Figure 7. An updated model of the vocal CPG. (A) Our results support the hypothesis that motor neuron collaterals form a cholinergic synapse onto interneurons in the motor nucleus that project to the premotor nucleus. These are likely inhibitory neurons, and are hypothesized to synapse directly onto FTNs in DTAM. (B) According to our model, inactivating motor neurons eliminates the feedback inhibition pathway (indicated by dashed lines). (C)

Hypothetical membrane potentials of FTNs in which the feedback signal is intact (black line) or disrupted (gray
line). In the intact circuit, FTN spikes are following by IPSPs (shaded area). In the absence of the feedback signal
(via transection, motor neuron silencing, or cholinergic antagonist), IPSPs no longer follow spikes, inducing
increased firing rates. (D) Hypothetical membrane potentials of three FTNs in an intact brain. In this scenario, spike
synchrony is ensured by motor neuron-dependent IPSPs, leading to entrained patterns of post-inhibitory rebound.
(E) Membrane potentials of three hypothetical FTNs in which feedback inhibition is eliminated. When FTNs no
longer receive simultaneous IPSPs, spikes are no longer entrained, and each cell generates a faster spike train
without temporal coordination between neurons.



Vocal motor nucleus n.IX-X

